ARMY RESEARCH LABORATORY

Mitigating Excessive Drying From the Use of Observations in Mesoscale Modeling

by Brian P. Reen, Robert E. Dumais, Jr., and Jeffrey E. Passner

ARL-TR-6775 **January 2014**

NOTICES

Disclaimers

The findings in this report are not to be construed as an official Department of the Army position unless so designated by other authorized documents.

Citation of manufacturer's or trade names does not constitute an official endorsement or approval of the use thereof.

Destroy this report when it is no longer needed. Do not return it to the originator.

Army Research Laboratory
Adelphi, MD 20783-1197

ARL-TR-6775 **January 2014**

Mitigating Excessive Drying From the Use of Observations in Mesoscale Modeling

Brian P. Reen, Robert E. Dumais, Jr., and Jeffrey E. Passner
Computational and Information Sciences Directorate, ARL

REPORT DOCUMENTATION PAGE

Form Approved
OMB No. 0704-0188

PLEASE DO NOT RETURN YOUR FORM TO THE ABOVE ADDRESS.

1. **REPORT DATE** *(DD-MM-YYYY)*	**2. REPORT TYPE**	**3. DATES COVERED (From - To)**
January 2014	Final	15 August 2012–30 September 2013

4. TITLE AND SUBTITLE

Mitigating Excessive Drying From the Use of Observations in Mesoscale Modeling

5a. CONTRACT NUMBER

5b. GRANT NUMBER

5c. PROGRAM ELEMENT NUMBER

6. AUTHOR(S)

Brian P. Reen,[*†] Robert E. Dumais, Jr.,[*] and Jeffrey E. Passner[*]

5d. PROJECT NUMBER

5e. TASK NUMBER

5f. WORK UNIT NUMBER

7. PERFORMING ORGANIZATION NAME(S) AND ADDRESS(ES)

U.S. Army Research Laboratory
ATTN: RDRL-CIE-M
2800 Powder Mill Road
Adelphi MD 20783-1197

8. PERFORMING ORGANIZATION REPORT NUMBER

ARL-TR-6775

9. SPONSORING/MONITORING AGENCY NAME(S) AND ADDRESS(ES)

10. SPONSOR/MONITOR'S ACRONYM(S)

11. SPONSOR/MONITOR'S REPORT NUMBER(S)

12. DISTRIBUTION/AVAILABILITY STATEMENT

Approved for public release; distribution unlimited.

13. SUPPLEMENTARY NOTES

[*]Battlefield Environment Division, U.S. Army Research Laboratory
[†]National Research Council Postdoctoral Associate, U.S. Army Research Laboratory

14. ABSTRACT

Observations can be used to enhance mesoscale model forecasts both through creation of an initial condition analysis and through application of observations over a period of time within the model. Because observations are not available at the same density as the model grid points, assumptions must be made regarding spatial and temporal correlations in order to apply the observations to the model. Methods are developed that mitigate overly dry model conditions caused by these assumptions.

The Weather Research and Forecasting model is applied to five cases centered over southern California to demonstrate the overdrying caused by incorporation of observations in the initial conditions, both at a discrete time and over a preforecast data assimilation period. Very dry conditions result from the assumption that model moisture error at the observation location is correlated with model moisture error at other locations in the model without regard to the relative magnitude of the moisture at those two locations. Modifications that account for this difference in the magnitude of moisture are made to both the initial condition analysis and the data assimilation methodology. These modifications greatly reduce the occurrence of excessive model dryness, while not degrading the overall model performance in predicting moisture.

15. SUBJECT TERMS

WRF, data assimilation, observation nudging, moisture

16. SECURITY CLASSIFICATION OF:			**17. LIMITATION OF ABSTRACT**	**18. NUMBER OF PAGES**	**19a. NAME OF RESPONSIBLE PERSON**
a. REPORT	**b. ABSTRACT**	**c. THIS PAGE**			Brian P. Reen
Unclassified	Unclassified	Unclassified	UU	33	**19b. TELEPHONE NUMBER** (*Include area code*) (301) 394-3072

Standard Form 298 (Rev. 8/98)
Prescribed by ANSI Std. Z39.18

Contents

List of Figures

List of Tables

Acknowledgments

AirDat LLC provided Tropospheric Aircraft Meteorological Data Reports (TAMDAR) observational data that expanded the above-surface data available for data assimilation and verification. This study was possible in part due to the data made available to the National Oceanic and Atmospheric Administration (NOAA) by various providers for inclusion in the Meteorological Assimilation Data Ingest System (MADIS). The Real Time Mesoscale Analysis (RTMA) use and reject lists were provided by Steve Levine at the National Weather Service's National Centers for Environmental Prediction – Environmental Modeling Center (NCEP-EMC) and greatly facilitated making full use of the MADIS observational dataset. The "madis2littler" tool was provided by Ruifang Li at the National Center for Atmospheric Research (NCAR). The first author was supported by a National Research Council postdoctoral associateship at the U.S. Army Research Laboratory (ARL) for part of this research.

1. Introduction

Observations are often used to enhance the initial conditions in a mesoscale model to improve the subsequent model forecast. However, in order to utilize observations made at discrete points to improve a three-dimensional model, one must make certain assumptions. We illustrate how the introduction of observations into the initial conditions can cause the initial conditions to be excessively dry, and demonstrate solutions to the overdrying.

Instead of directly using output from a coarser-grid model as initial conditions for a mesoscale model integration, incorporating observations into the initial conditions can allow the initial conditions to more closely match observed conditions. Various techniques are available to utilize observations in the initial conditions including those that introduce changes at discrete times (intermittent) and those that gradually adjust the model solution over many time steps (continuous). Examples of intermittent techniques include three-dimensional variational assimilation (3DVAR) and Ensemble Kalman filter, while examples of continuous techniques include four-dimensional variational assimilation (4DVAR) and Newtonian relaxation (nudging). Here we gradually nudge the model towards observations (observation nudging) during a preforecast in order to improve the conditions used to start the free forecast. This technique is conceptually simple, relatively inexpensive computationally, and allows the dynamic balance and intervariable consistency of the model to be maintained (Ardao-Berdejo and Stauffer, 1996; Seaman, 2000). Observation nudging has been used successfully in many past studies (e.g., Stauffer and Seaman, 1994; Schroeder et al., 2006; Otte, 2008a, b). We also use a flow-dependent multiscan Cressman analysis method to incorporate observations into the model conditions at the beginning of the preforecast.

Assimilation of moisture information can pose difficulties due to the high spatial variability of mixing ratio (and specific humidity) relative to the absolute value of mixing ratio (and specific humidity) (e.g., Dee and da Silva, 2003). This spatial variability may make it more difficult to determine the correlation length scales to assume when assimilating moisture. It may also mean that a rather modest error in mixing ratio at the observation location (as a percentage of the model mixing ratio) will be translated by the data assimilation methodology into a very large change in modeled mixing ratio (relative to the precorrected mixing ratio) at a nearby location.

We describe overdrying introduced into the model solution via incorporation of observations into the model initial conditions, and describe solutions to this issue. In section 2 we describe the model we used to investigate this problem and its configuration and in section 3 we describe the cases studied. The methodology used to incorporate observations is discussed in section 4, while the experimental design is included in section 5. Sections 6 and 7 describe the results and the summary and conclusions, respectively.

2. Model Description and Configuration

The Advanced Research version of the Weather Research and Forecasting model (WRF-ARW) v3.4.1 (Skamarock et al., 2008) was configured with 9-km horizontal resolution centered over southern California and 56 vertical layers. The model was integrated from 12 Coordinated Universal Time (UTC) to 12 UTC for the five case days described in section 3.

Global Forecast System (GFS) 0.5-degree horizontal resolution output is used to create initial conditions and boundary conditions. A higher-resolution product from the National Centers for Environmental Prediction, Marine Modeling and Analysis Branch, called the Real Time Global Sea Surface Temperature (Gemmill et al., 2007) has one-twelfth degree horizontal grid spacing and was used to specify sea surface temperatures. Where available, GFS snow fields were replaced with 1-km snow fields from the National Weather Service's National Operational Hydrologic Remote Sensing Center (NOHRSC) Snow Data Assimilation System (SNODAS) (National Operational Hydrologic Remote Sensing Center, 2004).

Obsgrid is part of the WRF software suite and can be used to create objective analyses and complete quality control on observations. Initial conditions for some experiments in this study are enhanced with observations using Obsgrid. Modifications to the methodology used to create these objective analyses are investigated in this study and described in section 4.4. We also use Obsgrid to perform quality control of the observations used for inclusion in the initial conditions and for data assimilation. The quality control component of Obsgrid includes checking observations for gross errors, comparing observations to nearby observations (buddy check), and comparing observations to a background field (here GFS). For moisture observations, in addition to checking relative humidity, buddy checks and checks against the background field were added for dewpoint to allow overly dry observations to be removed more efficiently.

The Mellor-Yamada-Janjić (MYJ) scheme (Janjić, 2002) is used to parameterize the atmospheric boundary layer. This parameterization predicts turbulent kinetic energy (TKE) and is a Mellor-Yamada Level 2.5 turbulence closure model. As in Lee et al. (2012) and Reen et al. (2013), the background TKE is decreased to better simulate conditions with low-TKE and the atmospheric boundary layer (ABL) depth diagnosis is altered. In preliminary experiments for this study, the standard MYJ scheme resulted in noisy TKE fields and thus noisy ABL depth fields over the water. These were resolved using the altered version of MYJ.

The WRF single-moment five-class microphysics parameterization (Hong et al., 2004; Hong and Lim, 2006) is utilized and the Kain-Fritsch cumulus parameterization (Kain, 2004) is utilized on the 9-km horizontal grid spacing domain only. For radiation, the Rapid Radiative Transfer Model (RRTM) (Mlawer et al., 1997) is used for longwave and the Dudhia scheme (Dudhia, 1989) for

shortwave. The Noah land surface model (Chen and Dudhia, 2001) is used to represent land surface processes.

The observation nudging capability of WRF (Deng et al., 2009) is used to incorporate observations into the model via a 6-hour (h) preforecast (12–18 UTC). During this preforecast, the model is gradually nudged towards observations of temperature, moisture, and wind. The standard WRFV3.4.1 observation nudging technique is described in more detail in section 4.3, as are modifications to this technique investigated here.

3. Case Description

Five 24-h periods from early 2012 over the southwestern United States were examined, which started at 12 UTC on 7 February, 9 February, 16 February, 1 March, and 5 March, 2013. The case days were chosen to include days with active weather and more benign weather. On 7 February a trough moved onshore and led to widespread precipitation in the region. More quiescent weather was in place for the 9 February case with a 500-hPa-ridge centered over central California at 12 UTC. On 16 February an upper-level low is near the California/Arizona border with Mexico at 12 UTC, bringing precipitation to that portion of the domain. The area of low pressure and the associated precipitation move off to the south and then east as the case day progresses. For
1 March, a weak shortwave trough results in precipitation in northern California at the beginning of the period that spreads to Nevada and then moves southward and decreases in coverage. There is widespread high-level cloudiness for the 5 March case due to weak upper-level low pressure, but very limited precipitation.

4. Methodology

4.1 Dewpoint Climatology

In order to provide an objective measure of whether the model is producing moisture fields that are unusually dry, and thus potentially suspect, a dewpoint climatology was constructed using rawinsonde data. All rawinsonde data for January, February, and March from 1990–2012 at four locations within the model domain are included. The four locations are Oakland, CA; San Diego, CA; Tucson, AZ; and Desert Rock, NV. Desert Rock did not take upper-air observations in 2011 or 2012. At each of the locations, the dewpoint representing the 0.1 percentile value was calculated for 50-hPa bins for the period described. For each 50-hPa bin, the lowest value for this 0.1 percentile value among the four locations was chosen to create a vertical profile of dewpoints. This vertical profile is used to evaluate whether the model is unrealistically dry. The 0.0 percentile value (the absolute minimum) was not used because that value would be more

sensitive to any erroneous values of dewpoint included in the observation dataset. For this comparison, dewpoint was calculated using Bolton (1980) for both the model and the observations. For the rawinsondes, dewpoint was first converted to water vapor mixing ratio using Hyland and Wexler (1983) to allow the use of Bolton (1980). The 0.1 percentile values are shown in figure 1.

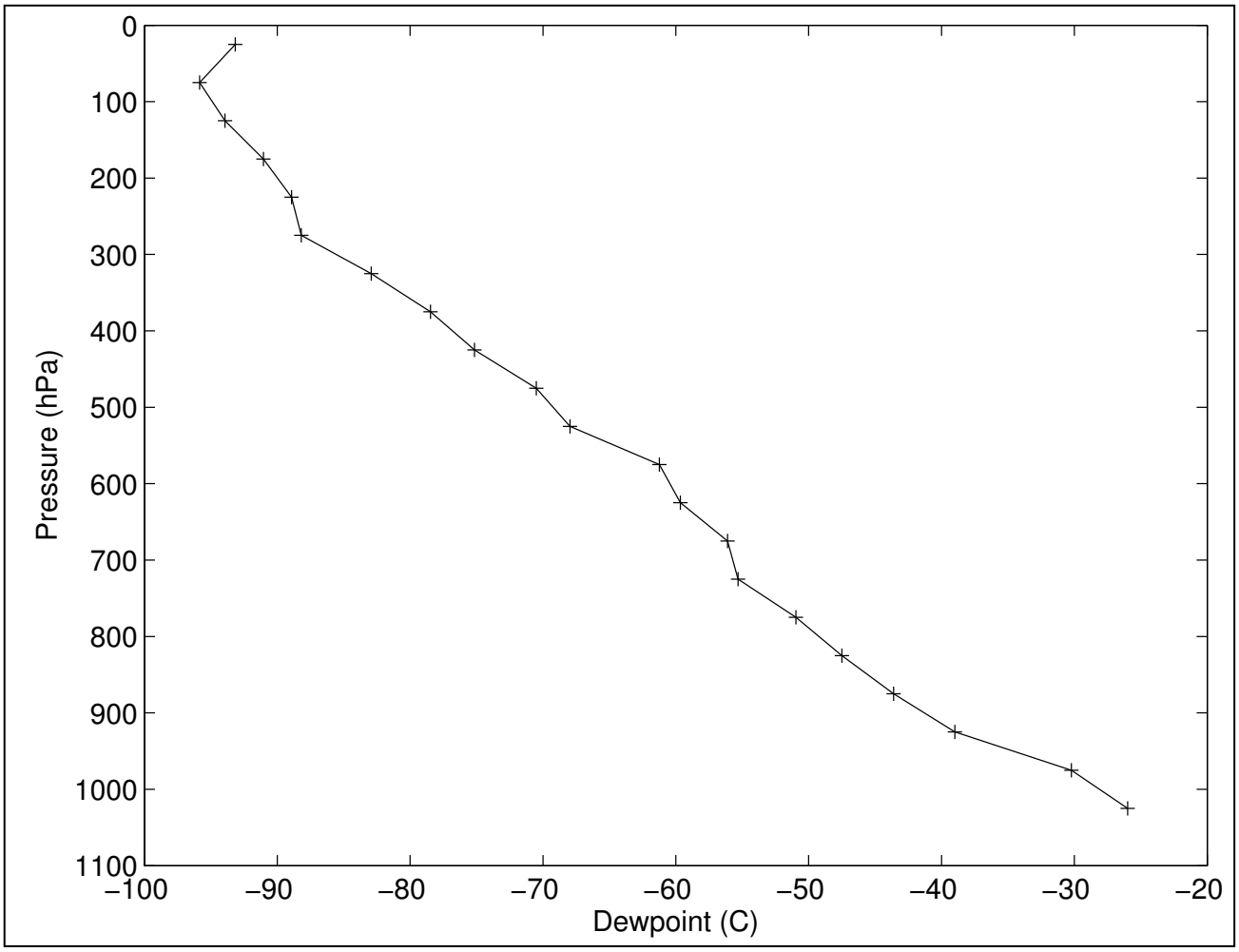

Figure 1. Vertical profile of the minimum of the 0.1 percentile dewpoint for Oakland, CA; San Diego, CA; Tucson, AZ; and Desert Rock, NV; for January–March, 1990–2012.

4.2 Observation Data Sources

Observations from the Meteorological Assimilation Data Ingest System (MADIS) (madis.noaa.gov) database as well as Tropospheric Aircraft Meteorological Data Reports (TAMDAR) (e.g., Gao et al., 2012) observations were used for data assimilation. The MADIS data included standard surface observations, as well as mesonet data, profiler data, aircraft data, and rawinsondes. In addition to the Obsgrid quality control procedures described in section 2, use/reject lists from a test version of the Real Time Mesoscale Analysis (RTMA) (De Pondeca et

al., 2011) were used to filter the mesonet data. The construction of these use/reject lists includes calculating the long-term differences between a given location's observations and a background field, and then comparing these differences to those found by comparing Aviation Routine Weather Report (METAR) observations (i.e., nonmesonet observations that should be well sited) to the background field. The goal of this process is to find stations whose observation differences from the background field are sufficiently larger than those of METAR observations that the mesonet observations are considered to not be trustworthy. Universal reject lists as well as separate day/night reject lists are used for temperature and moisture. For wind, mesonet observations are rejected unless they are on the universal accept list or the observed wind direction is within a wind direction bin that is listed as acceptable for that station. The wind direction bins allow wind observations to be included from a site where nearby obstructions only affect the wind observations when the wind is coming from certain directions. The use of these use/reject lists is designed to maximize the positive impact of mesonet observations while minimizing the potential negative impact of mesonet observations that may arise due to issues such as siting (e.g., wind observations at heights other than 10-m above ground level (AGL), obstructions near the observation location). The TAMDAR dataset consists of aircraft-based observations of temperature, moisture, and winds. TAMDAR is not included in MADIS during the study period, and is potentially more valuable than some other aircraft-based measurements due to its inclusion of moisture and its use of Global Positioning System (GPS)-based height rather than pressure altitude.

4.3 Nudging Technique

Observation nudging adds a nonphysical term to the tendency equations, and is implemented in WRF as

$$\frac{\partial q\mu}{\partial t}(x,y,z,t) = F_q(x,y,z,t) + \mu G_q \frac{\sum_{i=1}^{N} W_q^2(i,x,y,z,t)\left[q_o(i) - q_m(x_i,y_i,z_i,t)\right]}{\sum_{i=1}^{N} W_q(i,x,y,z,t)} \quad (1)$$

where q is the quantity being nudged (e.g., water vapor mixing ratio), μ is the dry hydrostatic pressure, F_q represents the physical tendency terms of q, G_q is the nudging strength for q, N is the total number of observations, i is the index to the current observation, W_q is the spatiotemporal weighting function, q_o is the observed value of q, and $q_m(x_i,y_i,z_i,t)$ is the model value of q interpolated to the observation location. The quantity q_o-q_m is the innovation. In WRF observation nudging, the innovations from surface observations are spread along the model surface, whereas innovations from above-surface observations are spread based on pressure. Note that unlike the standard WRF observation nudging code, surface observations reported as part of a sounding are treated as surface observations by the observation nudging rather than as part of the sounding; this allows them to be spread horizontally as surface observations.

We test placing a limit on the magnitude of negative water vapor mixing ratio innovations in certain conditions. Given an observation at a location A, an innovation will be calculated that is valid at location A in the model. The limit on the magnitude of negative water vapor mixing ratio innovations applies when the innovation from location A is applied to a location B and the model is drier at location B than at location A. In this case, the magnitude of the negative moisture innovation applied to location B is limited to be no more than the model water vapor mixing ratio at the location B. Consider the case where one is applying an observation $q_0(i)$ to $q_m(x,y,z,t)$.

If

$$\left\{\left[q_o(i) - q_m(x_i, y_i, z_i, t)\right] < 0\right\} \text{and} \left\{q_m(x, y, z, t) < q_m(x_i, y_i, z_i, t)\right\} \tag{2}$$

then the nudging equation becomes,

$$\frac{\partial q\mu}{\partial t}(x, y, z, t) = F_q(x, y, z, t) + \mu G_q \frac{\sum_{i=1}^{N} W_q^2(i, x, y, z, t) \max\left\{\left[q_o(i) - q_m(x_i, y_i, z_i, t)\right], -q_m(x, y, z, t)\right\}}{\sum_{i=1}^{N} W_q(i, x, y, z, t)} \tag{3}$$

4.4 Initial Condition Enhancement

For some experiments we use initial conditions generated by incorporating observations onto the GFS fields through a modified Cressman analysis with Obsgrid. The Cressman analysis is applied through a series of four scans with successively smaller radii of influence. The area a given wind or moisture observation influences is a "banana" shape following the wind flow (this reduces to an ellipse in noncurved flow and a circle in weak-wind conditions).

We investigate modifying the Cressman analysis in Obsgrid for relative humidity to limit its introduction of very dry conditions. The modification is applied in the following situation: when an observation at point A ($RH_{ob,A}$) indicates that the current first guess field ($RH_{fg,A}$) is too moist (i.e., $RH_{fg,A} > RH_{ob,A}$) and one is applying this correction (i.e., $RH_{ob,A}$ - $RH_{fg,A}$) to a point B where the first guess field ($RH_{fg,B}$) is drier than at point A (i.e., $RH_{fg,B} < RH_{fg,A}$). In this situation, the adjustment made to the first-guess field at point B to find the analysis value ($RH_{an,B}$) is scaled by the relationship between first-guess relative humidity at point B as compared to first-guess relative humidity at point A. In other words, for a case with a single observation at point A, when applying this to the analysis at point B, if

$$\begin{gathered} \left(RH_{fg,A} > RH_{ob,A}\right) \wedge \left(RH_{fg,B} > RH_{fg,A}\right) \\ \left(RH_{fg,A} > RH_{ob,A}\right) \wedge \left(RH_{fg,B} < RH_{fg,A}\right) \end{gathered} \tag{4}$$

then,

$$RH_{an,B} = RH_{fg,B} + F * \left(\frac{RH_{fg,B}}{RH_{fg,A}} \right) \left(RH_{ob,A} - RH_{fg,A} \right)$$

$$RH_{an,B} = RH_{fg,B} + F * \left(\frac{RH_{fg,B}}{RH_{fg,A}} \right) \left(RH_{ob,A} - RH_{fg,A} \right) \quad (5)$$

Else,

$$RH_{an,B} = RH_{fg,B} + F * \left(RH_{ob,A} - RH_{fg,A} \right) RH_{an,B} = RH_{fg,B} + F * \left(RH_{ob,A} - RH_{fg,A} \right) \quad (6)$$

where *F* is the distance weighting. For the first scan (largest radius of influence), the first-guess field is GFS, but for subsequent scans the first-guess field is the end result of the previous scan.

5. Experimental Design

A set of experiments that varies the initial conditions and the data-assimilation configuration are compared to a control experiment using GFS data as initial conditions and no data assimilation (Exp. Control). These experiments were completed on all five case days and are listed in table 1.

Table 1. Experimental design.
The table indicates whether the source of initial conditions is GFS and whether observations are incorporated via objective analysis and whether modifications are made to the Cressman method for moisture. The table also indicates whether nudging is applied, whether the nudging method was modified for moisture, and the nudging weight.

Experiment Name	Initial Conditions			Nudging		
	GFS	Obs	Cressman Modified	Applied	Modified	Weight (*G*)
Control	X					
ObIC	X	X				
ObIC+	X	X	X			
ObIC+Nud4	X	X	X	X		4×10^{-4} s^{-1}
ObIC+Nud4+	X	X	X	X	X	4×10^{-4} s^{-1}
ObIC+Nud8	X	X	X	X		8×10^{-4} s^{-1}
ObIC+Nud8+	X	X	X	X	X	8×10^{-4} s^{-1}

The initial conditions were created using three options. Exp. Control used the GFS fields for the initial conditions. The standard Cressman analysis scheme in Obsgrid was used to create the initial conditions for Exp. ObIC. Exp. ObIC+ also included observations in the initial conditions, but did so using the modification to the Cressman scheme for moisture described in section 4.4. All experiments not described in this paragraph also used this modification.

Data assimilation was applied via observation nudging for some experiments, but with two variations among these experiments. The standard technique was used for Exp. ObIC+Nud4 and

ObIC+Nud8, while the modification to water vapor mixing ratio assimilation described in section 4.3 was used for Exp. ObIC+Nud4+ and ObIC+Nud8+. The nudging weight (G), was set to 4×10^{-4} s^{-1} for Exp. ObIC+Nud4 and ObIC+Nud4+, but to 8×10^{-4} s^{-1} for Exp. ObIC+Nud8 and ObIC+Nud8+.

6. Results

6.1 Initial Conditions

Unusually dry conditions can be introduced into WRF through the initial conditions. For example, figure 3a shows the dewpoint at model level 15 at the initial time (12 UTC) for Exp. Control on 16 February 2012. Using the GFS data alone for initial conditions yields one area with very dry conditions over the Pacific Ocean (at approximately 29 °N, 122 °W); the minimum dewpoint in this area is approximately –78 °C. This is well below the climatological 0.1 percentile value of –47 °C for this level (approximately 850 hPa; figure 1) derived as described in section 4.1.

The inclusion of observations in the initial condition analysis via Obsgrid (Exp. ObIC) results in more extensive dry regions (figure 3b). A much larger area of relatively low dewpoints are now found along the western edge of the domain. Also, now there are two additional areas with low dewpoints: (1) over the Pacific Ocean at about 33 °N, 122 °W where the minimum dewpoint is approximately –78 °C at approximately 850 hPa; (2) along the Arizona-Mexico border around 111 °W where the minimum dewpoint is approximately –80 °C at approximately 700 hPa. For this model level at this time the percentage of grid cells whose dewpoint falls below the climatological 0.l percentile value increases with the inclusion of observations in the initial conditions (i.e., Exp. Control to Exp. ObIC) from 1.13% to 8.50%.

The overall scope of the problem can be examined by looking at the percent of model grid points below 350 hPa that have a dewpoint less than the 0.1 percentile value (figure 4). Model grid points above 350 hPa are excluded due to the very dry conditions at these levels (the climatological 0.1 percentile value falls below –80 °C, just above 350 hPa). For Exp. Control (figure 4a), the time series of this quantity indicates that most of the experiments stay below 0.2%, but that 16 February starts out around 0.5% and then falls. This means that some points are initialized with very dry dewpoints when using GFS, but the prevalence of these dry locations is higher for the 16 February case. Incorporating observations into the initial conditions via Obsgrid (figure 4b) notably increases the percentage of very dry model grid points; all experiments start out at or above about 0.5%, but 16 February starts out above 1.5%. Note that for all experiments the prevalence of dry model grid points decreases with time.

Incorporating the altered analysis scheme for the relative humidity field described in section 4.4 allows one to gain the benefits of incorporating observations in the initial conditions while not

introducing the very dry spots found with the standard analysis technique. First, consider the 16 February case where including observations into the initial conditions resulted in notable drying on model level 15 and the formation of two additional very dry spots. The altered analysis scheme (Exp. ObIC+) results in the removal of all very dry spots (figure 3); the domain minimum dewpoint is now approximately –48 °C instead of –80 °C as with Exp. ObIC. Note that the structure of the dewpoint field at this level in Exp. ObIC+ matches the structure of Exp. ObIC better than it matches Exp. Control, with the major difference being the lack of very dry conditions in Exp. ObIC+. The domain mean time series of grid points below 350 hPa for Exp. ObIC+ (figure 4c) shows that very few of the model grid points are less than the 0.1 percentile value (less than 0.1%); comparing this to the standard analysis method (Exp. ObIC; figure 4b) demonstrates the ability of the altered analysis scheme to greatly minimize very dry conditions in the initial conditions.

Comparison of these experiments to observations (figure 5) indicates that although modifying the moisture analysis technique to avoid overdrying may slightly degrade how well the analysis fits the observations above 1000-m AGL, during the forecast the model performs at least as well (or slightly better) than when using the original method. At the initial time (12 UTC), inclusion of observations in the analysis (Exp. ObIC compared to Exp. Control) improves dewpoint mean absolute error (MAE) at all three levels plotted: by 2.3 K at 0–12000 m (figure 5a), by 1.3 K at 0–1000 m (figure 5d), and by 0.8 K at 2 m (figure 5g). Modification of the analysis technique (Exp. ObIC+ compared to Exp. ObIC) changes the mean fit-to-observations by less than 0.1 K, except in the 0–12000-m-AGL layer where MAE increases by 0.2 K, although it still retains over 90% of the improvement gained by including observations in the analysis. During the first six hours of the model integration including observations in the analysis improves the forecast at 2 m (0.3 K in figure 5h) and 0–1000-m AGL (0.1 K in figure 5e), but degrades the forecast at 0–12000 m (0.2 K in figure 5b). However, modification of the analysis method slightly improves dewpoint above the surface for 13–18 UTC (by 0.1K for both 0–1000 and 0–12000-m AGL). Thus, when compared to not performing an analysis, use of the new analysis method yields a slight degradation at 0–12000 m (0.1 K in figure 5b), but improvements for both 0–1000-m AGL (0.2 K in figure 5e) and 2 m (0.3 K in figure 5h). For the 7–24 h forecast (19–12 UTC) the three initial conditions yield nearly identical dewpoint MAE (figure 5c, f, i). Overall, the new moisture analysis methodology slightly improves model dewpoint forecasts as compared to the original moisture methodology.

6.2 Data Assimilation

When observation nudging is used in combination with the altered analysis methodology for creating observation-enhanced initial conditions the model appears to produce areas that are unrealistically dry. An example of this is figure 6d, which shows the dewpoint from Exp. ObsIC+Nud8 on 1 March at 13 UTC at model level 16. There is an area with very low dewpoints just offshore of southern California (at this location model level 16 is approximately 825 hPa, 1600-m MSL). In the middle of this area, model water vapor mixing ratios drop to zero. The

absence of the dry spot from the analogous experiment without data assimilation (Exp. ObsIC+; figure 6a) indicates that the observation nudging is contributing to this dry spot.

Further investigation reveals that the 12 UTC San Diego rawinsonde is the specific observation that leads to the dry spot. Around 825 hPa, the model indicates a smoother decrease of dewpoint with height than the sharp decrease in the observation (figure 2). This appears to the main cause of a negative moisture innovation, which causes the model to be nudged towards a drier solution at this point, as expected. The appearance of cloud water by 13 UTC in the non-nudging experiment in the vicinity of San Diego indicates that the physical tendency terms are working to increase the moisture at this point, contrary to the nudging. Therefore, compared to a case where the physical tendency terms are zero, the data assimilation is less effective in decreasing the error, and thus the innovation does not decrease as rapidly with time and the nudging tendency term will not decrease as rapidly with time. Just to the west of San Diego, the model does not form clouds by 13 UTC, suggesting that the model may be less resistant to drying there. The innovation is calculated at San Diego, where the physical tendency terms work to counteract the drying from nudging during this period. The innovation is then applied to an area that includes the area west of San Diego, where the physical tendency terms do not counteract drying during this period. The data assimilation is thus able to remove all moisture in a limited area west of San Diego at this model level by 13 UTC.

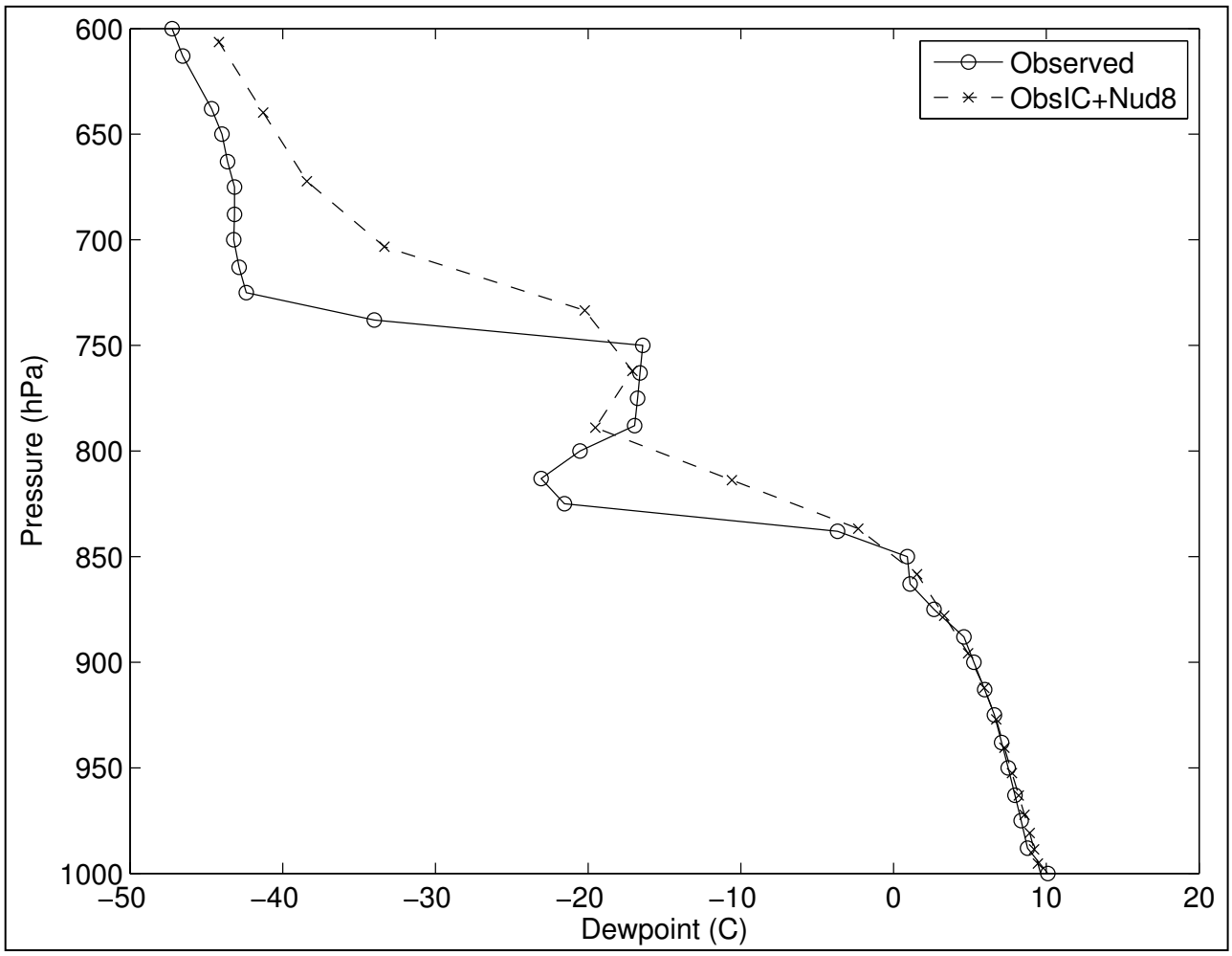

Figure 2. Vertical profile comparing dewpoint from the 12 UTC 1 March 2012 San Diego, CA, rawinsonde as provided to the data assimilation after quality control is applied to the WRF model dewpoint at the grid point closest to this location for Exp. ObsIC+Nud8.

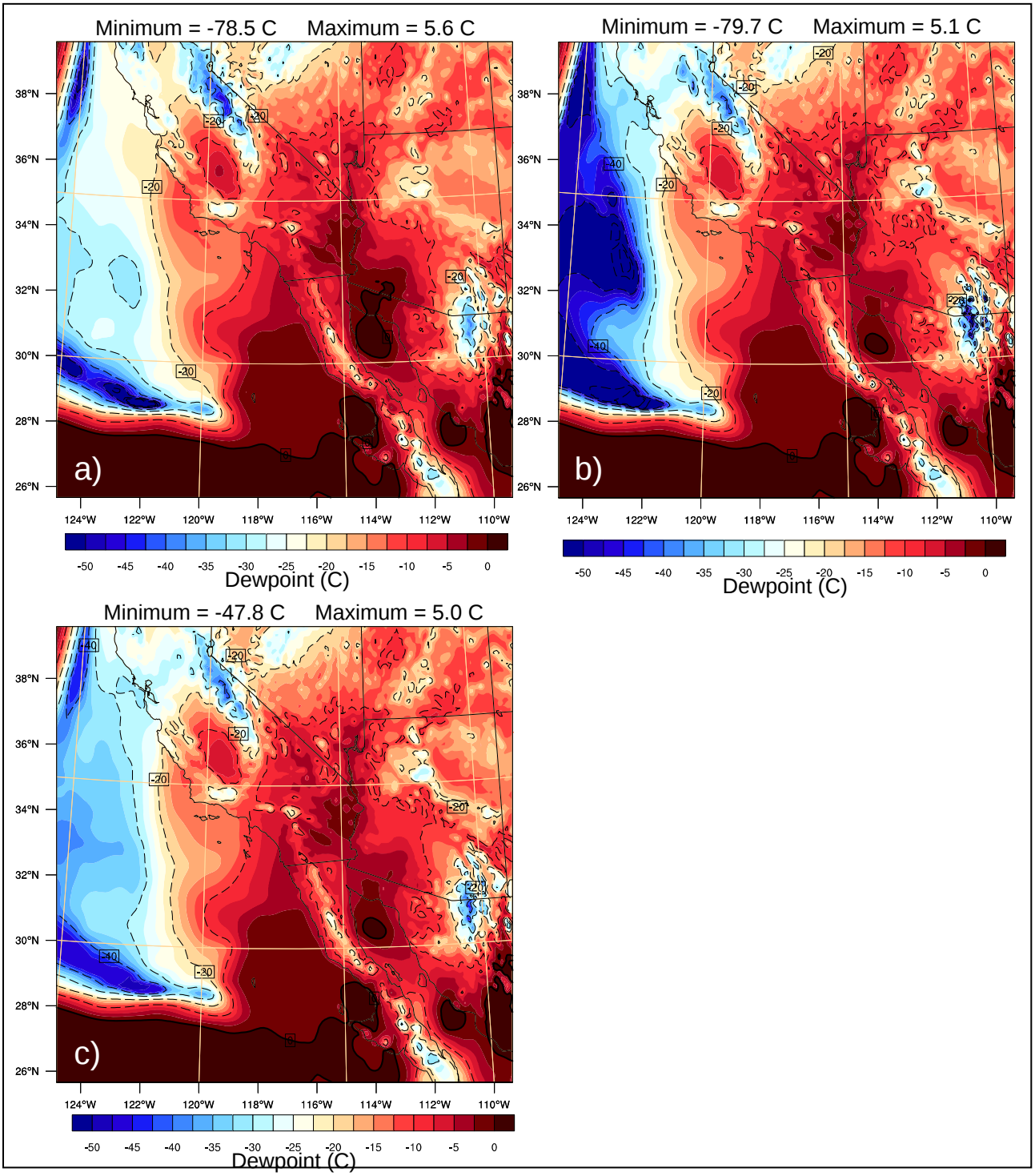

Figure 3. Dewpoint (°C) for Exps. (a) Control, (b) ObsIC, and (c) ObsIC+ on 16 February at 12 UTC at WRF-ARW model level 15.

Dewpoint is indicated by shading, but note that all values less than –50 °C are shaded as –50 °C for clarity. Contours are also shown for every 10 °C increment of dewpoint, with those for negative values dashed. The minimum and maximum dewpoints across the domain at this time and model level are indicated at the top of the figure.

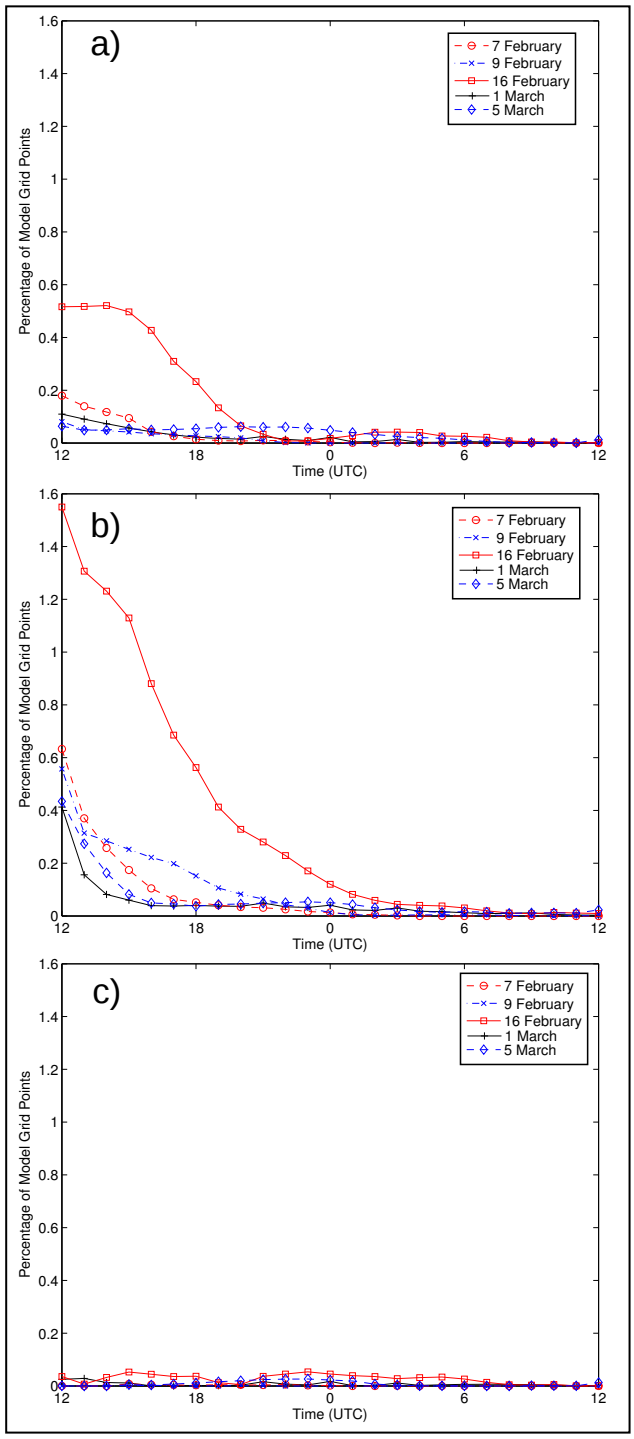

Figure 4. Time series of the percentage of WRF grid points below 350 hPa that fall below the 0.1 percentile climatological value for that pressure bin for Exps. (a) Control, (b) ObIC, and (c) ObIC+.

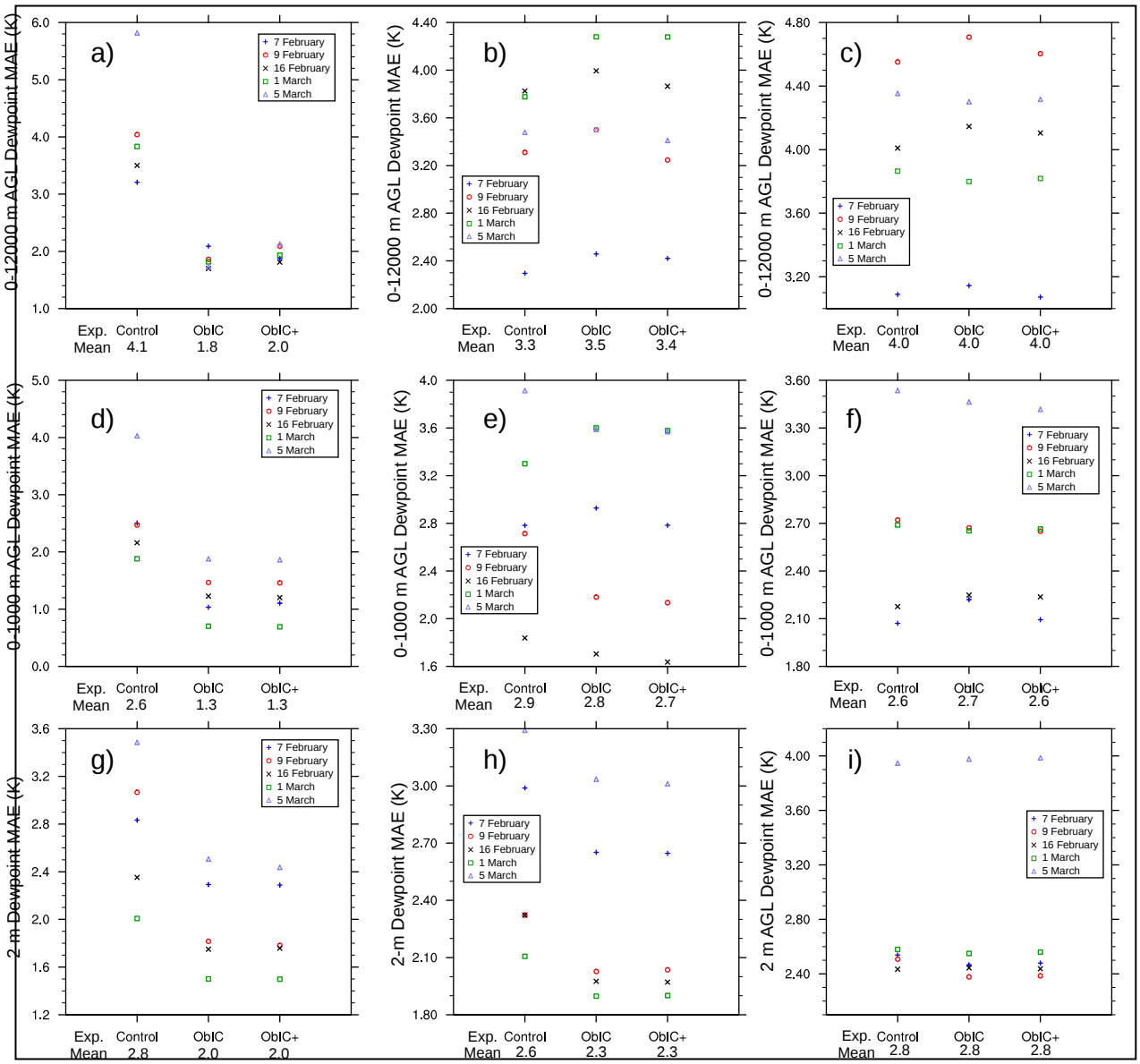

Figure 5. Dewpoint MAE for (a–c) 0–12000-m AGL; (d–f) 0–1000-m AGL; and (g–i) 2-m AGL at (a, d, g) 12 UTC, (b, e, h) 13–18 UTC, and (c, f, i) 19–12 UTC for Exps. Control, ObIC, and ObIC+ for all five case days.
Note: The dewpoint MAE averaged over all five case days is noted under the experiment name on the x-axis.

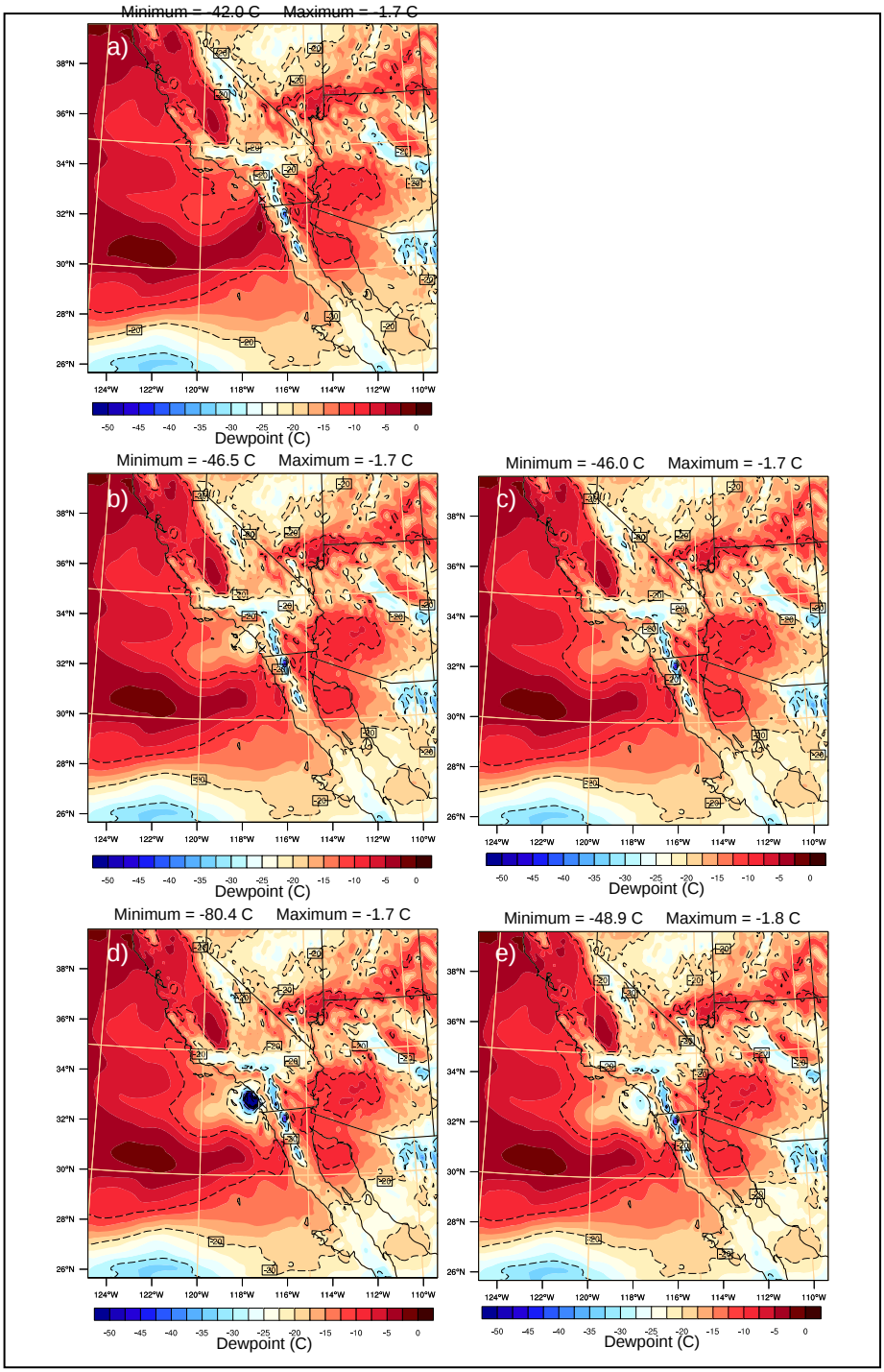

Figure 6. Dewpoint (°C) for Exps. (a) ObIC+, (b) ObIC+Nud4, (c) ObIC+Nud4+, (d) ObsIC+Nud8, and (e) ObsIC+Nud8+ on 1 March at 13 UTC at model level 16.

Note: All values < –50 °C are shaded in the same dark blue. The plotting routine treats all dewpoints less than approximately –80 °C as –80 °C, which prevents "singularities" where the water vapor mixing ratio goes to or approaches zero. Black contour lines are plotted every 10 °C; these lines are dashed for negative values. The black "X" on the eastern edge of the dry spot marks the San Diego, CA, rawinsonde location.

Figure 7c shows a time series of the percentage of Exp. ObIC+Nud8 model grid points below 350 hPa that had dewpoints lower than the 0.1 percentile value from the dewpoint climatology. The day with the dry spot we already indicated was due to nudging (1 March) and 16 February have the largest percentage of "dry" grid points, but the other three case days also have gridpoints that meet the criterion. For all five case days, the percentage of dry points does not increase after the end of the data assimilation (18 UTC), consistent with data assimilation being a primary cause of the dry spots. For the initial conditions, among the five case days the percentage of grid points below the 0.1 percentile criteria ranges from 0.00%–0.04%, consistent with the initial condition creation no longer being a significant source of very dry conditions for these experiments.

Because observation nudging is causing the bulk of the remaining excessively dry areas in the WRF experiments, the first potential solution we explore is decreasing the influence of observation nudging on the solution by decreasing the strength of the observation nudging. The strength of the observation nudging is determined by the observation nudging weight; this term represents the inverse e-folding time for the decrease of the difference between the model and the observation at the observation location (i.e., the innovation). The nudging weight in the observation nudging experiment with the very dry area west of San Diego is 8×10^{-4} s^{-1}, which translates to an e-folding time of 21 minutes (min) for the innovation. When the nudging weight is decreased by half to 4×10^{-4} s^{-1}, the very dry area just west of San Diego is no longer present at 13 UTC (Exp. ObIC+Nud4, figure 6b). Compared to the experiment without any nudging (Exp. ObIC+, figure 6a), the model is drier just west of San Diego—but the extreme dryness predicted with the stronger nudging weight is absent.

The overall distribution of sub-0.1 percentile dewpoints below 350 hPa for the five case days (figure 7) indicates that the weaker nudging strength is not sufficient to completely resolve the excessive dryness introduced by observation nudging. The percent of WRF grid points dryer than the 0.1 percentile value decreases with the decrease in nudging weight (figure 7a, c); however, the 1 March and 16 February cases still peak at more than 0.4% of grid points being dryer than the dewpoint threshold.

Observation nudging assumes that the tendency term introduced by nudging is not larger than the physical tendency terms; this should allow the model to ingest the observation while keeping a meteorologically consistent solution. The efficacy of reducing the nudging weight in reducing model predictions of very dry conditions suggests that with the stronger nudging we may be violating this assumption.

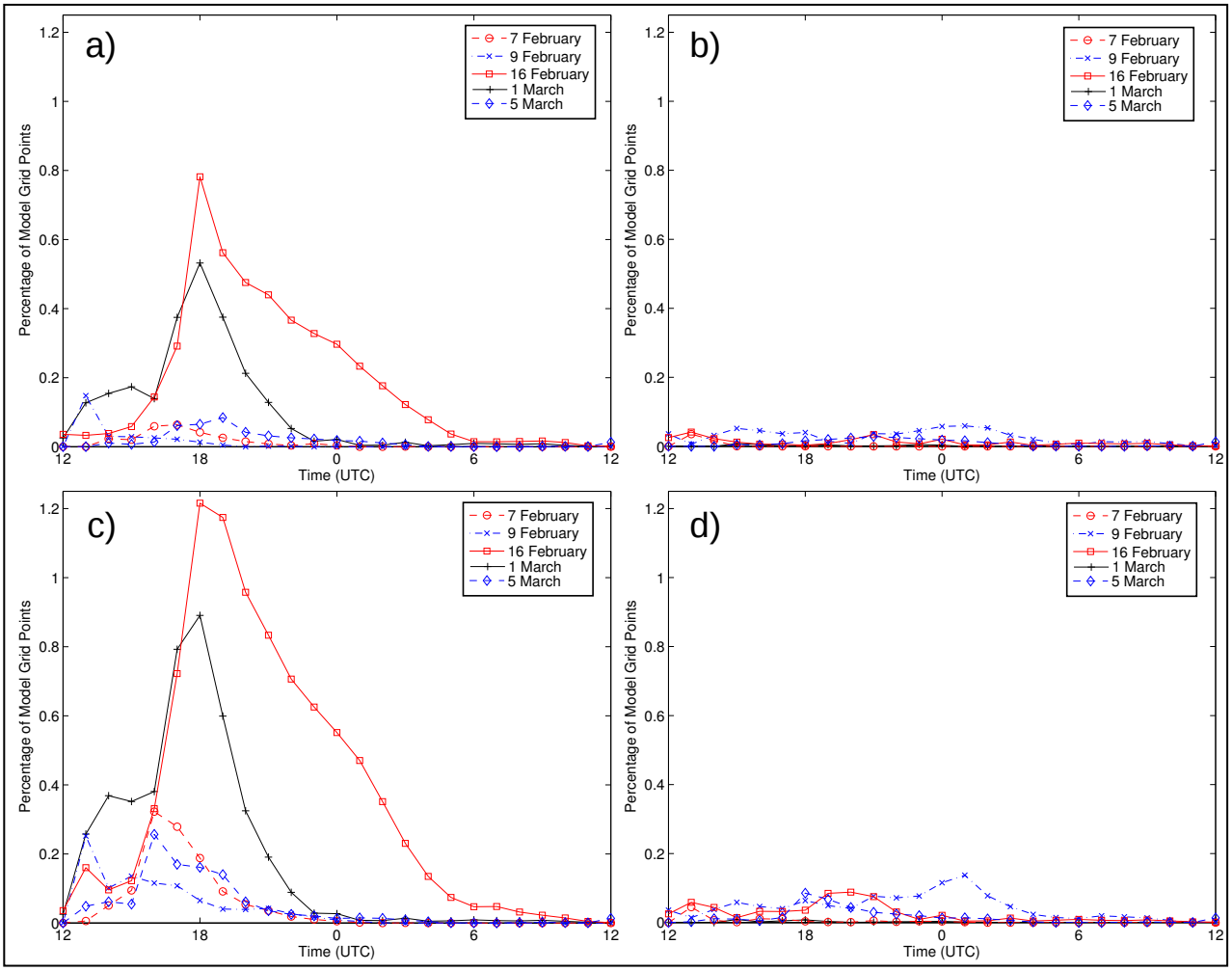

Figure 7. Time series of the percentage of WRF grid points below 350 hPa that fall below the 0.1 percentile climatological value for that pressure bin for Exps. (a) ObIC+Nud4, (b) ObIC+Nud4+, (c) ObIC+Nud8, and (d) ObIC+Nud8+.

However, water vapor mixing ratio differs from the other two nudged variables, namely potential temperature and winds. Unlike potential temperature, spatial variability in water vapor mixing ratio at a given vertical level is large compared to its magnitude. While the wind field shares this characteristic with water vapor mixing ratio, unlike water vapor mixing ratio it is not meteorologically problematic to have either—or both—of the wind components (u and v) zero, or even negative. Additionally, it may be that it is more difficult for physical tendency terms to prevent observation nudging from drying the model solution excessively than it is for nudging to introduce meteorologically inconsistent results for other variables. Except near the land surface, it is not clear which moisture tendency terms would effectively prevent unrealistically dry conditions from being introduced by observation nudging. Therefore, compared to the other nudged variables, moisture is uniquely exposed to the possibility of observation nudging introducing values that are sufficiently low to be physically unrealistic.

To address this issue, the modification to observation nudging described in section 4.3 is applied to both the experiment with the weaker nudging (Exp. ObIC+Nud4) and the experiment with the stronger nudging (Exp. ObIC+Nud8). In the area west of San Diego that was very dry at 13 UTC in Exp. ObIC+Nud8 (figure 6d), the observation nudging modification (Exp. ObIC+Nud8+, figure 6e) results in much moister conditions, while allowing the overall dewpoint field to remain very similar to Exp. ObIC+Nud8. For the weaker nudging—even with the standard technique (Exp. ObIC+Nud4, figure 6b)—there was not an excessively dry area west of San Diego, but the new technique (Exp. ObIC+Nud4+, figure 6c) decreases the drying that did occur in that location, while keeping the overall dewpoint field very similar. Examining the statistics for all model grid points below 350 hPa, the new technique reduces the percentage of points with dewpoint below the 0.1 percentile to below 0.2% for all experiments (figure 7).

Verification of model dewpoint against observations indicates that observation nudging improves the model results, while the modification to the observation nudging technique for moisture has limited effect on overall dewpoint MAE (figure 8). Excluding the initial conditions, during the preforecast time period 13–18 UTC (figures 8a, d, and g) the use of observation nudging decreases dewpoint MAE for the 2-m diagnostic level, as well as in the 0–1000 and 0–12000-m AGL layers. During this period where observation nudging is being applied there appears to be a small advantage to stronger nudging (ObsIC+Nud4 vs. ObsIC+Nud8) while the modification to the observation nudging technique (compare ObsIC+Nud4 vs. ObsIC+Nud4+ and compare ObsIC+Nud8 vs. ObsIC+Nud8+) has little effect on the verification, except for a small improvement in the 0–1000-m-AGL layer with the strong nudging (ObIC+Nud8 vs. ObIC+Nud8+ in figure 8d). For the 6 h after the preforecast (19–00 UTC, figures 8b, e, and h) the addition of nudging is generally advantageous, but both nudging strengths perform similarly. The observation nudging methodology change generally has little effect on the overall dewpoint MAE, but there is a slight improvement in the 0–12000-m-AGL layer with the stronger nudging (ObIC+Nud8 vs. ObIC+Nud8+ in figure 8b). Later in the forecast (01–12 UTC, figures 8c, f, and i), as expected there is less difference in dewpoint verification among the experiments. The use of nudging does improve 0–1000-m AGL dewpoint (ObIC+ vs. ObIC+Nud4 in figure 8f) and the use of the weaker nudging does improve 2-m AGL dewpoint (ObIC+ versus ObIC+Nud4 in figure 8i). There is no indication that the modification to the moisture nudging methodology adversely affects overall WRF dewpoint predictions, and the modification may slightly improve overall model dewpoint predictions.

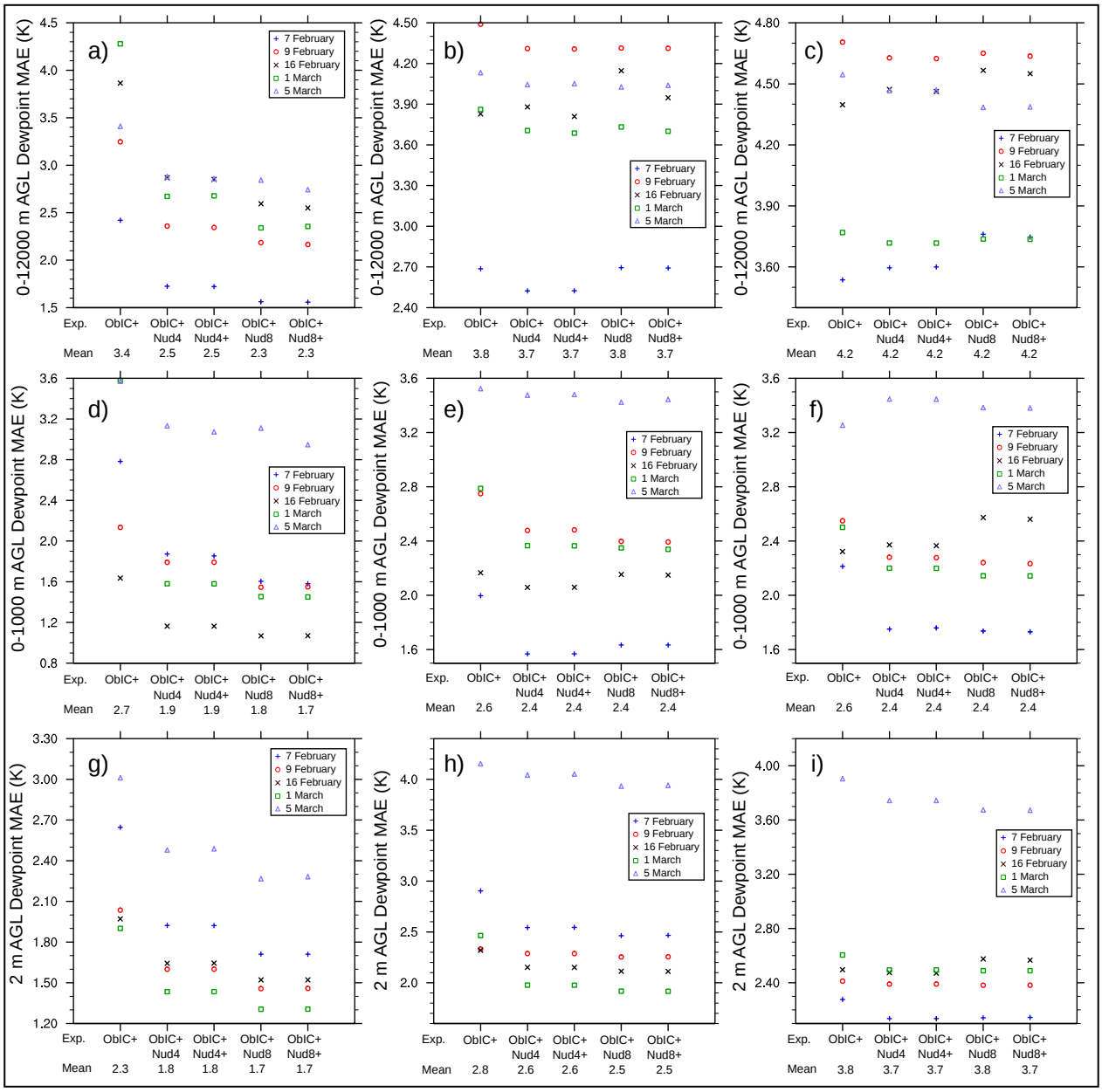

Figure 8. Dewpoint MAE for (a–c) 0–12000-m AGL; (d–f) 0–1000-m AGL; and (g–i) 2-m AGL at (a, d, g) 13–18 UTC, (b, e, h) 19–00 UTC, and (c, f, i) 01–12 UTC for Exps. ObIC+, ObIC+Nud4, ObIC+Nud4+, ObIC+Nud8, and ObIC+Nud8+ for all five case days.

Note: The dewpoint MAE averaged over all five case days is noted under the experiment name on the x-axis.

7. Summary and Conclusions

Conditions that appear to be excessively dry can be introduced into a mesoscale model via analysis techniques, which incorporate observations in the initial conditions at a given time as

well as via observation nudging data assimilation—which applies observations over some time period. WRF-ARW was used for five case days (7 February, 9 February, 16 February, 1 March, and 5 March 2012) to examine this issue over the southwestern United States. A dewpoint climatology was calculated using the rawinsonde observations available within a 23-year period from four locations within the model domain for January–March and this climatology was used to objectively determine if the model value was "too dry"; in each 50 hPa pressure bin the lowest 0.1-percentile value among the locations was used to construct a 0.1-percentile value that was used as the criterion determining excessive dryness.

The creation of initial conditions by combining a first guess field from GFS with observations via a modified Cressman analysis was found to increase the prevalence of very low moisture; a method to resolve this issue was demonstrated. The case of 16 February 2012 was used to illustrate this issue. The percentage of model grid points in the initial conditions below the 0.1-percentile value ranges among the case days from 0.06%–0.52% without the Cressman analysis, but increases to range between 0.41%–1.55% with the Cressman analysis. The Cressman analysis was altered such that if the analysis was decreasing relative humidity at a location where the first guess was dryer than the model at the observation location, then the decrease would be scaled by the ratio between model relative humidity at the location being dried and model relative humidity at the location of the observation that is causing the drying. This removed the creation of excessive drying by the analysis of observations onto the GFS fields; it decreased the percentage of model grid points that are very dry to range between 0.00%–0.04%. Dewpoint verification indicates that use of the altered method for inclusion of observations in the initial conditions slightly decreases the fit of the initial conditions to observations above 1000 m (MAE increases by 0.2 K) compared to the original method; however, 90% of the increase in fit from the original analysis methodology is retained. For the model forecast, during the first 6 h the model-predicted dewpoint slightly improves with the new analysis as compared to the original method, while after the first 6 h the change in methodologies has very little effect on the verification. The modification in the analysis methodology is effective in removing the very dry conditions introduced by the original analysis methodology while not negatively impacting the overall model dewpoint forecast.

The use of observation nudging was also found to introduce areas of excessive dryness, especially with stronger application of the nudging; a method was found to alleviate this issue. An example of this drying was seen on 1 March 2012 where in 1 h nudging decreased the water vapor mixing ratio to zero at approximately 825 hPa in an area over the Pacific Ocean, due to nudging based on the 12 UTC San Diego rawinsonde. Overall, at the end of the preforecast period (18 UTC), the percentage of model grid points with dewpoints below the 0.1-percentile threshold ranges among the case days from 0.01%– 0.78%, with 4×10^{-4} s^{-1} weighting and 0.07%–1.22%, with 8×10^{-4} s^{-1} weighting. To mitigate this issue, negative water vapor mixing ratio innovations for observation nudging are limited to have an absolute magnitude less than the model water vapor mixing ratio at the point at which the innovation is being applied. This greatly

decreases the incidence of very dry areas in the model; at the end of the preforecast period, the percentage of model grid points with dewpoints below the 0.1-percentile threshold range among the case days from 0.00%–0.02% (4×10^{-4} s^{-1}), or from 0.01%–0.09% (8×10^{-4} s^{-1}). Dewpoint verification indicates that the new methodology does not degrade modeled dewpoint, and may slightly improve the dewpoint output by WRF-ARW. The modified moisture observation nudging methodology notably decreases the introduction of very low water vapor levels by observation nudging, while the modification does not degrade the overall model moisture predictions.

Applying both the modification to the relative humidity analysis methodology and the modification to the water vapor mixing ratio observation nudging in concert with modifications to the MYJ TKE parameterization largely eliminates excessively dry conditions from the WRF solution. These modifications do not degrade the overall model dewpoint forecast. In addition to the modifications, applying the observation nudging more weakly (4×10^{-4} s^{-1} rather than 8×10^{-4} s^{-1}) also mitigates the formation of very dry areas. Quality control of moisture observations is also important for ensuring that observations do not cause excessively dry model conditions.

8. References

Ardao-Berdejo, J.; Stauffer, D. R. On the Relative Contribution of the Newtonian Relaxation Term in a Nonhydrostatic Mesoscale Model Used for Dynamic Analysis. In: *11th AMS Conference on Numerical Weather Prediction*, Norfolk, VA, USA, pp 200–202, 1996.

Bolton, D. The Computation of Equivalent Potential Temperature. *Mon. Wea. Rev.*, **1980**, *180*, 1046–1053.

Chen, F.; Dudhia, J. Coupling an Advanced Land-Surface/Hydrology Model with the Penn State/NCAR MM5 Modeling System. Part I: Model Description and Implementation. *Mon. Wea. Rev.* **2001**, *129*, 569–585.

Dee, D. P.; da Silva, A. M. The Choice of Variable for Atmospheric Moisture Analysis. *Mon. Wea. Rev.* **2003**, *131*, 155–171.

Deng, A.; Stauffer, D.; Gaudet, B.; Dudhia, J.; Bruyere, C.; Wu, W.; Vandenberghe, F.; Lui, Y.; Bourgeois, A. Update on WRF-ARW End-to-End Multi-Scale FDDA System. 10th WRF Users' Workshop, NCAR, 23–26 June, Boulder, CO. 1.9. pp. 14, 2009.

De Pondeca, M. S. F. V. and Coauthors: The Real-Time Mesoscale Analysis at NOAA's National Centers for Environmental Prediction: Current Status and Development. *Wea. Forecasting* **2011**, *26*, 593–612.

Dudhia, J. Numerical Study of Convection Observed During the Winter Monsoon Experiment Using a Mesoscale Two-Dimensional Model. *J. Atmos. Sci.* **1989**, *46*, 3077–3107.

Gao, Feng; Zhang, Xiaoyan; Jacobs, Neil A.; Huang, Xiang-Yu; Zhang, Xin; Childs, Peter P. Estimation of TAMDAR Observational Error and Assimilation Experiments. *Wea. Forecasting* **2012**, *27*, 856–877.

Gemmill, W.; Katz, B.; Li, X. Daily Real-Time, Global Sea Surface Temperature – High-Resolution Analysis: RTG_SST_HR. NOAA/NWS/NCEP/MMAB Office Note 260, 39 pp, 2007. Available online at http://polar.ncep.noaa.gov/mmab/papers/tn260/MMAB260.pdf. (accessed December 6, 2013).

Hong, S. -Y.; Dudhia, J.; Chen, S. -H. Chen. A Revised Approach to Ice Microphysical Processes for the Bulk Parameterization of Clouds and Precipitation. *Mon. Wea. Rev.* **2004**, *132*, 103–120.

Hong, S. -Y.; Lim, J. -O. J. The WRF Single-Moment 6-class microphysics scheme (WSM6). *Journal of the Korean Meteorological Society* **2006**, *42*, 129–151.

Hyland, R. W.; Wexler, A. Formulations for the Thermodynamic Properties of the Saturated Phases of H2O from 173.15K to 473.15K, ASHRAE Trans, **89(2A)**, 500–519, 1983.

Janjić, Z. I. Nonsingular Implementation of the Mellor–Yamada Level 2.5 Scheme in the NCEP Meso model, *NCEP Office Note*, No. 437, 61 pp, 2002.

Kain, J. S. The Kain-Fritsch Convective Parameterization: An Update. *J. Appl. Meteor*. **2004**, *43*, 170–181.

Mlawer, E. J.; Taubman, S. J.; Brown, P. D.; Iacono, M. J.; Clough, S. A. Radiative Transfer for Inhomogeneous Atmosphere: RRTM, a Validated Correlated-k Model for the Long-Wave. *J. Geophys. Res.* **1997**, *102* **(D14)**, 16663–16682.

National Operational Hydrologic Remote Sensing Center, 2004. *Snow Data Assimilation System (SNODAS) Data Products at NSIDC*. Boulder, CO USA: National Snow and Ice Data Center. http://dx.doi.org/10.7265/N5TB14TC (accessed December 6, 2013).

Otte, T. L. The Impact of Nudging in the Meteorological Model for Retrospective Air Quality Simulations. Part I: Evaluation Against National Observation Networks. *J. Appl. Meteorol. Climatol.* **2008a**, *47*, 1853–1867.

Otte, T. L. 2008b: The Impact of Nudging in the Meteorological Model for Retrospective Air Quality Simulations. Part II: Evaluating Collocated Meteorological and Air Quality Observations. *J. Appl. Meteorol. Climatol.* **2008b**, *47*, 1868–1887.

Reen, B. P.; Schmehl, K. J.; Young, G. S.; Lee, J. A.; Haupt, S. E.; Stauffer, D. R. Uncertainty in Contaminant Concentration Fields Resulting from Planetary Boundary Layer Depth Uncertainty. Submitted to *J. Appl. Meteorol. Climatol*, **2013**.

Schroeder, A. J.; Stauffer, D. R.; Seaman, N. L.; Deng, A.; Gibbs, A. M.; Hunter, G. K.; Young, G. S. Evaluation of a High-Resolution, Rapidly Relocatable Meteorological Nowcasting and Prediction System. *Mon. Weather Rev.* **2006**, *134*, 1237–1265.

Seaman, N. L. Meteorological Modeling for Air-Quality Assessments. *Atmos. Environ.* **2000**, *34*: 2231–2259.

Skamarock, W. C.; Klemp, J. B.; Dudhia, J.; Gill, D. O.; Barker, D. M.; Duda, M. G.; Huang, X. -Y.; Wang, W.; Powers, J. G. A Description of the Advanced Research WRF version 3, NCAR Tech. Note NCAR/TN-475+STR, National Center for Atmospheric Sciences, Boulder, CO, USA, 125 pp, 2008.

Stauffer, D. R.; Seaman, N. L. Multiscale Four-Dimensional Data Assimilation. *J. Appl. Meteorol.* **1994**, *33*: 416–434.

9. List of Symbols, Abbreviations, and Acronyms

3DVAR	three-dimensional variational assimilation
4DVAR	four-dimensional variational assimilation
ABL	atmospheric boundary layer
AGL	above ground level
ARL	U.S. Army Research Laboratory
GFS	Global Forecast System
GPS	Global Positioning System
h	hour
MADIS	Meteorological Assimilation Data Ingest System
MAE	mean absolute error
METAR	aviation routine weather report
min	minute
MYJ	Mellor-Yamada-Janjić
NCAR	National Center for Atmospheric Research
NCEP-EMC	National Centers for Environmental Predictions Environmental Modeling Center
NOHRSC	National Operational Hydrologic Remote Sensing Center
NOAA	National Oceanic and Atmospheric Administration
RRTM	Rapid Radiative Transfer Model
RTMA	Real Time Mesoscale Analysis
SNODAS	Snow Data Assimilation System
TAMDAR	Tropospheric Aircraft Meteorological Data Reports
TKE	turbulent kinetic energy
UTC	Coordinated Universal Time

WRF-ARW	Advanced Research Version of the Weather Research and Forecasting Model

NO. OF COPIES	ORGANIZATION
1 (PDF)	DEFENSE TECHNICAL INFORMATION CTR DTIC OCA
2 (PDFS)	DIRECTOR US ARMY RSRCH LAB RDRL CIO LL RDRL IMAL HRA RECORDS MGMT
1 (PDF)	GOVT PRINTG OFC A MALHOTRA
1 (PDF)	DIR USARL RDRL CIE M B REEN R DUMAIS J PASSNER